Dept. of Mech. Eng.
CUET

Published Online March 2015 (http://www.cuet.ac.bd/merj/index.html)

Mechanical Engineering Research Journal

Vol. 9, pp. 72–78, 2013

ISSN: 1990-5491

DEVELOPMENT OF A MATHEMATICAL MODEL BASED ON THE DYNAMICS OF A WHEELED SKID-STEERED UGV

R. I. Rousseau[1*] and C. Ha[2]

[1]Institute of Energy Technology, Chittagong University of Engineering & Technology, Chittagong-4349, Bangladesh

[2]Aerospace Engineering Division, School of Mechanical Engineering, University of Ulsan, Republic of Korea

Abstract: Mobile robots using skid-steering technique are very popular for terrain navigation because of their robust mechanical structure and highly reliable mechanism. In order to ensure safe operations of skid-steering unmanned ground vehicles (UGVs), it is essential to understand the vehicle-terrain interaction. This paper aims to give a general and unifying presentation on the mathematical modeling of wheeled type skid-steered UGV in the presence of wheel skidding and slipping. The model is developed based on the dynamics working on the UGV including skidding as well as slipping effects. Kinematic and dynamic model of the UGV is first presented followed by the development of a pseudo-static friction model. The friction model is then simplified for theoretical aspects in order to analyze the wheel-ground interaction along with the UGV motion. Responses of the simulation are investigated to check the effectiveness of the model behavior as well as to check the system stability for terrain navigation.

Keywords: *Skid-steering mechanism, UGV, Slip, Robot dynamics, Trajectory tracking.*

1. INTRODUCTION

Unmanned ground vehicles (UGVs) have too many potential applications, both in military and civil areas, such as reconnaissance, surveillance, target acquisition, and rescue. Now many UGVs, especially in military applications, use skid-steering for all-terrain mobility, both in tracked and wheeled platforms. The absence of a steering system for a skid-steered UGV makes the vehicle mechanically robust and simple for terrain or outdoor environment navigation. Due to the varying tire-ground interactions and over constrained contact, it is quite challenging to obtain accurate dynamic models for such mobile robots. These UGVs need to be tested under different conditions before putting into work. It is very important to model the actual vehicle and simulate test conditions similar to those robots that might encounter while developing or testing the robot. Vehicle dynamics accommodates all forms of conveyance using rubber tired vehicles, track laying vehicles, trains etc. The control of the UGVs only at the kinematic level is not sufficient as there are many works which were based only on the kinematic models, and gave less satisfactory responses. Use of the dynamic models can provide better results on the trajectory tracking performance of UGVs.

Despite of having so many inconveniences, it is really challenging to get correct dynamic models and trajectory tracking performance for such UGVs because of the varying tire/ground interactions and over constrained contact.

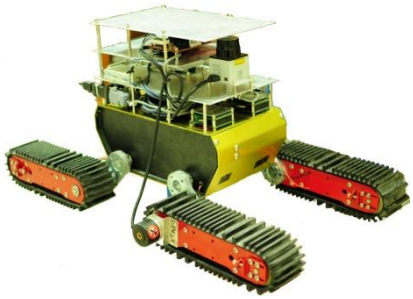

Fig. 1: A four wheeled skid-steered UGV.

Skidding and slipping effects of wheels make the kinematic and dynamic modeling of the skid-steered UGVs very complicated. In [1], Shiller et al. determine the nominal track forces required to follow a specified path at desired speeds and compute vehicle

[*] **Corresponding author:** Email: iftekharrousseau@gmail.com; Tel: +8801782-681868

orientations along the path that are consistent with the nonholonomic constraint. Zhang et al. [2] derive a simplified dynamic model which is adequate for control design and treat the remaining terms as model uncertainty. In [3], a path tracking control algorithm for tracked surface drilling machines is presented by Ahmadi et al. in which the general dynamic model of vehicle is simulated including track-soil interactions. In [4], a trajectory tracking control problem for a four-wheel differentially driven mobile robot moving is considered by Caracciolo et al. on an outdoor terrain. Wang et al. [5] develop a trajectory planning algorithm for a four-wheel-steering vehicle based on vehicle kinematics in which the flexibility offered by the steering is utilized fully in the trajectory planning. In [6], a mathematical model of a 4-wheel skid-steering mobile robot is presented by Kozłowski et al. in a systematic way where the robot is considered as a subsystem consisting of kinematic, dynamic and drives levels. In [7], Jingang et al. again present localization and slip estimation scheme for a skid-steered mobile robot using low-cost inertial measurement units (IMU). They again present an adaptive trajectory control design for a skid-steered wheeled mobile robot with kinematic and dynamic modeling of the robot [8]. Later, Wang et al. in [9] aim to give a general and unifying presentation on modeling of wheeled mobile robots in the presence of wheel skidding and slipping from the perspective of control design. In [10], a comparison study is presented for the control performance of an omni-directional mobile robot with and without considering wheel slip. It was found that the significance of slip increases when the wheel/ground friction coefficient is larger. A tire/road friction model in automotive study was also considered for the longitudinal friction force.

In this paper, primarily the kinematic and dynamic modeling of a wheeled skid-steered UGV are discussed in section 2. Section 3 describes a pseudo-static friction model for the wheel-ground interaction. The responses of the trajectory tracking are demonstrated in section 4. Finally, we discuss the effectiveness of the model and conclude the paper with future research directions in section 5.

2. KINEMATIC AND DYNAMIC MODEL

We consider the following assumptions without loss of generality.

Modeling Assumptions

1. Mass center is located at the geometric center of the body frame.
2. Point contact between wheel and ground.
3. Contact rolling resistance force is negligible.
4. Two wheels on each side rotate at same speed.
5. Wheel slipping and skidding is considered.
6. Equally distributed normal forces at the wheel/ground contact points among four wheels during motion.
7. Robot is running on a flat ground surface and four wheels always in contact with ground surface.

Figure 2 represents the schematic of the wheeled skid-steered UGV according to which a fixed reference or global frame is defined as (*X, Y*) and a moving body or local frame as (*x*, y).

Let the wheel angular velocities be ω_i and the velocities of the wheel contact points be u_i, i = 1, 2, 3, 4, for the left-front, left-rear, right-front, and right-rear wheels, respectively. According to the assumption 4, $\omega_1 = \omega_2$ and $\omega_3 = \omega_4$. The longitudinal and lateral forces at each wheel's contact point are F_i and P_i, i = 1, 2, 3, 4, respectively. The velocity of the robot mass center is denoted as v_G. Also the longitudinal and lateral wheel bases are represented as *L* and *W*, respectively.

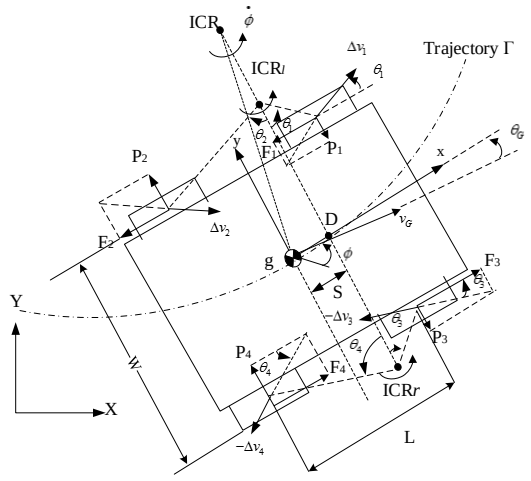

Fig. 2: Top view schematic of a wheeled skid-steered UGV on a flat surface.

Let the instantaneous center of rotation (ICR) of the left-side wheel contact points, right-side wheel contact points, and the robot body as ICR_l, ICR_r, and ICR_g, respectively. It is known that ICR_l, ICR_r and ICR_g lie on a line parallel to the *y*-axis [8]. Let $\dot{x}, \dot{y}, \dot{\phi}$ be the longitudinal, lateral and angular velocity of the vehicle in the body frame respectively. The absolute velocities in global frame are

$$\begin{bmatrix} \dot{X} \\ \dot{Y} \end{bmatrix} = \begin{bmatrix} \cos\phi & -\sin\phi \\ \sin\phi & \cos\phi \end{bmatrix} \begin{bmatrix} \dot{x} \\ \dot{y} \end{bmatrix} = R^T(\phi) \begin{bmatrix} \dot{x} \\ \dot{y} \end{bmatrix}$$

Differentiation with respect to time

$$\begin{bmatrix} \ddot{X} \\ \ddot{Y} \end{bmatrix} = R^T(\theta) \begin{bmatrix} \ddot{x} - \dot{y}\dot{\theta} \\ \ddot{y} + \dot{x}\dot{\theta} \end{bmatrix}$$

Longitudinal velocities of the wheel/ground contact points are

$$u_{1x} = u_{2x} = \dot{x} - \frac{W}{2}\dot{\phi},\ u_{3x} = u_{4x} = \dot{x} + \frac{W}{2}\dot{\phi} \qquad (1)$$

where *r* = wheel radius. Then we can define the longitudinal wheel slips λ_i as

$$\lambda_i = \frac{r\omega_i - u_{ix}}{r\omega_i} = -\frac{\Delta u_{ix}}{r\omega_i} \qquad (2)$$

where $\Delta u_{ix} = u_{ix} - r\omega_i$. Note that $\lambda_1 = \lambda_2$ and $\lambda_3 = \lambda_4$ according to assumption 4. Under the above definition, $\lambda \in [0, 1]$ if the wheel is under traction, and $\lambda \in (-\infty, 0]$ if the wheel is under braking, which is undesirable for uniformly modeling the wheel/ground friction under traction and braking cases. In order to avoid such a problem, we restrict the magnitude of λ to a maximum magnitude of 1.0 for $\lambda < 0$ under braking [8].

Let the x-y coordinates for ICR_l, ICR_r, and ICR_g be (x_l,y_l), (x_r,y_r), and (x_g,y_g), respectively. We can find that the x-coordinate S of the ICRs satisfies the following constraints

$$S = x_l = x_r = x_g = -\frac{\dot{y}}{\dot{\phi}} \tag{3}$$

The longitudinal skid velocities of the wheel/ground contact points are

$$\Delta u_{1x} = \Delta u_{2x} = (y_l - \frac{W}{2})\dot{\phi}$$
$$\Delta u_{3x} = \Delta u_{4x} = (y_l + \frac{W}{2})\dot{\phi} \tag{4}$$

Combining (1), (4) and $\Delta v_{ix} = v_{ix} - r\omega_i$, we get

$$y_l = \frac{\dot{x} - r\omega_1}{\dot{\phi}}; y_r = \frac{\dot{x} - r\omega_3}{\dot{\phi}} \text{ and } y_g = \frac{\dot{x}}{\dot{\phi}} \tag{5}$$

3. FRICTION MODELING

In order to develop a friction model we consider the longitudinal friction forces $F_i = N_i\mu_i$ where i = 1, 2, 3, 4; μ_i = friction coefficient; and N_i = normal force. Coefficient μ is a function of the longitudinal slip λ. Figure 3(a) shows the μ-λ curve that is obtained by fitting the experimental data [11]. Here, a linear approximation of the μ-λ curve is considered as shown in Fig. 3(b). For the traction case, the friction coefficient μ can be approximated by the following functions.

$$\mu(\lambda) = \begin{cases} K\lambda & \lambda \in [0, \lambda_m] \\ K\lambda_m - \dfrac{K\lambda_m - \mu_s}{1-\lambda_m}(\lambda - \lambda_m) & \lambda \in [0, \lambda_m] \end{cases} \tag{6}$$

where K = friction stiffness coefficient, λ_m = longitudinal slip value corresponding to the maximum wheel/ground friction coefficient, and μ_s = longitudinal wheel/ground sliding friction coefficient.

Assume, μ_s is a fraction of the pick friction coefficient μ_p, i.e.

$$\mu_s = \alpha\mu_p = \alpha K\lambda_m \qquad \text{(where, } 0 \le \alpha \le 1\text{)}$$

After simplification, equation (6) becomes

$$\mu(\lambda) = K[\sigma_1(\lambda) + \sigma_2(\lambda)\,\mathrm{sgn}(\lambda)\lambda] \tag{7}$$

where function sgn(x) = 1 if $x \ge 0$ and function sgn(x) = -1 if $x <$ 0. In case of traction

$$\sigma_1(\lambda) = \begin{cases} 0 & 0 \le \lambda < \lambda_m \\ \dfrac{1-\alpha\lambda_m}{1-\lambda_m}\lambda_m & \lambda \ge \lambda_m \end{cases}$$
$$\sigma_2(\lambda) = \begin{cases} 1 & 0 \le \lambda < \lambda_m \\ -\dfrac{1-\alpha}{1-\lambda_m}\lambda_m & \lambda \ge \lambda_m \end{cases} \tag{8}$$

and for the braking case

$$\sigma_1(\lambda) = \begin{cases} 0 & -\lambda_m < \lambda \le 0 \\ -\dfrac{1-\alpha\lambda_m}{1-\lambda_m}\lambda_m & \lambda \le -\lambda_m \end{cases}$$
$$\sigma_2(\lambda) = \begin{cases} 1 & -\lambda_m < \lambda \le 0 \\ \dfrac{1-\alpha}{1-\lambda_m}\lambda_m & \lambda \le -\lambda_m \end{cases} \tag{9}$$

Longitudinal friction force F_i and lateral friction force P_i are dependent on each other, and their magnitudes form a force circle [12] as

$$F_i = F_{ir}\cos\theta_i \text{ and } P_i = F_{ir}\sin\theta_i$$

where F_{ir} = resultant maximum friction force of the ith wheel and θ_i = slip angle at the ith wheel. The longitudinal friction force $F_i = N_i\mu_i(\lambda_i)$. Therefore, we can rewrite the lateral friction force P_i as

$$P_i = F_i \tan\theta_i \qquad (i = 1, 2, 3, 4) \tag{10}$$

The longitudinal forces F_i and the lateral forces P_i follow the relationship in Eq. (10). Figure shows the four combinations of friction forces for each side of wheels [8]. Denote the ICR coordinates as (x, y) and for all cases shown in Fig. we can rewrite Eq. (10) as follows.

$$P_1 = F_1\,\mathrm{sgn}(\lambda_1)\frac{\frac{L}{2} - x}{y} \text{ and } P_1 = F_1\,\mathrm{sgn}(\lambda_1)\frac{\frac{L}{2} - x}{y} \tag{11}$$

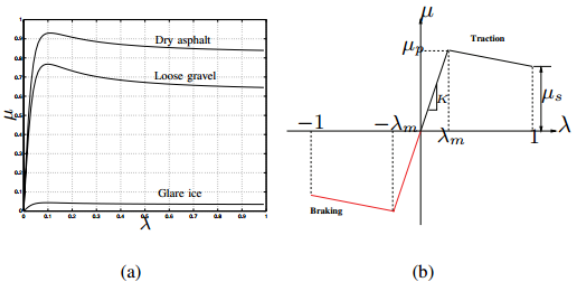

Fig. 3: (a) Relationship between μ and λ. (b) A linear approximation of the μ-λ relationship [8].

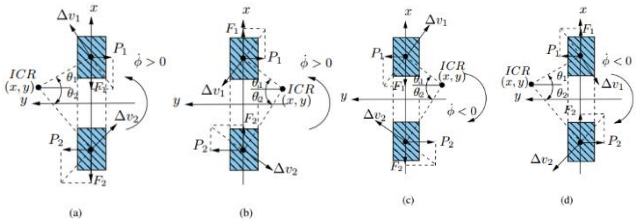

Fig. 4: Friction forces; (a) braking while turning left, (b) traction while turning left, (c) braking while turning right and (d) traction while turning right [8].

Notice that $y \neq 0$ and F_1, $F_2 \ge 0$ is the magnitude of the longitudinal friction force in the above equations. sgn (λ_1), sgn (λ_2) = +*ve* and –*ve* for traction and braking respectively. Assume normal load at each wheel $N_i = mg/4$ is a constant. The ground soil conditions are same four all the four wheels as the robot size

is relatively small. Therefore, $\lambda_1 = \lambda_2$, $\lambda_3 = \lambda_4$ and $F_1 = F_2$, $F_3 = F_4$. Using Eq. (11), we can get

$$P_1 = F_1 \operatorname{sgn}(\lambda_1)\frac{\frac{L}{2} - x_l}{y_l - \frac{W}{2}} \qquad P_2 = -F_1 \operatorname{sgn}(\lambda_1)\frac{\frac{L}{2} + x_l}{y_l - \frac{W}{2}} \tag{12}$$

$$P_3 = F_3 \operatorname{sgn}(\lambda_3)\frac{\frac{L}{2} - x_r}{y_r + \frac{W}{2}} \qquad P_3 = -F_3 \operatorname{sgn}(\lambda_3)\frac{\frac{L}{2} + x_r}{y_r + \frac{W}{2}} \tag{13}$$

Therefore, dynamic equations in the (x, y) frame are as follows

$$m\ddot{x} = F_1 \operatorname{sgn}(\lambda_1) + F_2 \operatorname{sgn}(\lambda_2) + F_3 \operatorname{sgn}(\lambda_3) + F_4 \operatorname{sgn}(\lambda_4)$$

$$\text{or, } m\ddot{x} = 2[F_1 \operatorname{sgn}(\lambda_1) + F_3 \operatorname{sgn}(\lambda_3)] \tag{14a}$$

$$m\ddot{y} = P_1 + P_2 + P_3 + P_4 \tag{14b}$$

$$I_g\ddot{\phi} = 2[-F_1 \operatorname{sgn}(\lambda_1) + F_3 \operatorname{sgn}(\lambda_3)]\frac{W}{2} - (-P_1 + P_2 - P_3 + P_4)\frac{L}{2} \tag{14c}$$

where m = mass of the UGV and I_g = mass moment of inertia of the UGV about g.

Traction/braking forces $F_i = N_i \mu_i(\lambda_i)$ is found using Eqs. (2), (4), (5), and (7) and we can obtain the friction force model as follows

$$F_1 = F_2 = \frac{mg}{4}K\sigma_1(\lambda_1) - \frac{mg}{4}K \operatorname{sgn}(\lambda_1)\sigma_2(\lambda_1)[(\dot{x} - \frac{W}{2}\dot{\phi})v_1 - 1]$$

$$F_3 = F_4 = \frac{mg}{4}K\sigma_1(\lambda_3) - \frac{mg}{4}K \operatorname{sgn}(\lambda_3)\sigma_2(\lambda_3)[(\dot{x} + \frac{W}{2}\dot{\phi})v_2 - 1] \tag{15}$$

Here $v_1 = 1/r\omega_1$ and $v_2 = 1/r\omega_3$

We define the control input variables as follows

$$v_1 = \sigma_2(\lambda_1)u_1 - \sigma_2(\lambda_3)u_2 \text{ and } v_2 = \sigma_2(\lambda_1)u_1 + \sigma_2(\lambda_3)u_2$$

The dynamics of the body frame (x, y) can be obtained using friction model (15) and Eq. (2) as

$$\ddot{x} = gK(\frac{1}{2}\sigma_\Sigma + \frac{1}{4}W\dot{\phi}v_1 - \frac{1}{2}\dot{x}v_2) \tag{16a}$$

$$\ddot{y} = -\frac{1}{2}gK\dot{y}[v_2(1 + \frac{1}{2}\sigma_{r2}) + \frac{1}{2}\sigma_{r1}v_1] \tag{16b}$$

$$\ddot{\phi} = \frac{mgK}{4I_G}\{-W\sigma_\Delta + (W\dot{x} - \frac{L^2}{4}\dot{\phi}\sigma_{r1})v_1 - \frac{1}{2}[\mathrm{W}^2 + L^2(1 + \frac{1}{2}\sigma_{r2})]\dot{\phi}v_2\} \tag{16c}$$

where, $\sigma_{r1} = \dfrac{\sigma_1(\lambda_1)\operatorname{sgn}(\lambda_1)}{\lambda_1\sigma_2(\lambda_1)} - \dfrac{\sigma_1(\lambda_3)\operatorname{sgn}(\lambda_3)}{\lambda_3\sigma_2(\lambda_3)}$;

$$\sigma_{r2} = \frac{\sigma_1(\lambda_1)\operatorname{sgn}(\lambda_1)}{\lambda_1\sigma_2(\lambda_1)} + \frac{\sigma_1(\lambda_3)\operatorname{sgn}(\lambda_3)}{\lambda_3\sigma_2(\lambda_3)}$$

and $\sigma_\Delta = \sigma_{1\Delta} + \sigma_{2\Delta}$; $\sigma_{1\Delta} = \sigma_1(\lambda_1)\operatorname{sgn}(\lambda_1) - \sigma_1(\lambda_3)\operatorname{sgn}(\lambda_3)$;

$\sigma_{2\Delta} = \sigma_2(\lambda_1) - \sigma_2(\lambda_3)$; $\sigma_\Sigma = \sigma_{1\Sigma} + \sigma_{2\Sigma}$; $\sigma_{1\Sigma} = \sigma_1(\lambda_1)\operatorname{sgn}(\lambda_1)$ $+\sigma_1(\lambda_3)\operatorname{sgn}(\lambda_3)$; $\sigma_{2\Sigma} = \sigma_2(\lambda_1) + \sigma_2(\lambda_3)$;

Now, we define generalized coordinates as $Q = [X\ Y\ \phi]^T$. Using Eq. (1), the body frame dynamics (16) can be transferred into global frame (X, Y) as

$$M\ddot{Q} + c(Q,\dot{Q}) = E(Q,\dot{Q}) \tag{17}$$

where, $u = [u_1 \quad u_2]^T$

$$M = \begin{bmatrix} m & 0 & 0 \\ 0 & m & 0 \\ 0 & 0 & Ig \end{bmatrix}; \qquad E(Q,\dot{Q}) = \frac{1}{4}mgK\begin{bmatrix} R^T E_1 \\ e_2 \end{bmatrix};$$

$$c(Q,\dot{Q}) = m\dot{\phi}\begin{bmatrix} 0 & 1 & 0 \\ -1 & 0 & 0 \\ 0 & 0 & 0 \end{bmatrix}\dot{q} - \frac{1}{4}mgK\begin{bmatrix} 2R^T\begin{bmatrix}\sigma_\Sigma \\ 0\end{bmatrix} \\ -W\sigma_\Delta \end{bmatrix};$$

$$E_1 = \begin{bmatrix} W\dot{\phi} & -2\dot{x} \\ -\sigma_{r1}\dot{y} & -2\dot{y}(1 + \frac{1}{2}\sigma_{r2}) \end{bmatrix};$$

$$e_2 = \left[W\dot{x} - \frac{1}{4}L^2\sigma_{r1}\dot{\phi} \quad -\frac{\dot{\phi}}{2}[\mathrm{W}^2 + L^2(1 + \frac{1}{2}\sigma_{r2})]\right]$$

Operative Nonholonomic Constraint

We have the nonholonomic constraint [Eq. (3)]. The x-axis projection of the ICR cannot be larger than $L/2$. Otherwise the UGV would skid along the y-axis thus losing control. In order to have the UGV move properly, it should have

$$\left|-\dot{y}/\dot{\phi}\right| < L/2$$

Therefore, we introduced the following operative constraint

$$\dot{y} + S\dot{\phi} = 0 \tag{18}$$

[where $0 < S < L/2$]

In term of generalized coordinates,

$$\begin{bmatrix} -\sin\phi & \cos\phi & S \end{bmatrix}\begin{bmatrix} \dot{X} \\ \dot{Y} \\ \dot{\phi} \end{bmatrix} = A(Q)\dot{Q} = 0 \tag{19}$$

where $A(Q) = \begin{bmatrix} -\sin\phi & \cos\phi & S \end{bmatrix}$

Incorporating this nonholonomic constraint into the dynamics [Eq. (14)], we got our reduced state-space model as follows

$$\dot{Q} = G(Q)\eta \tag{20a}$$

$$\dot{\eta} = (G^T(Q)MG(Q))^{-1}G^T(Q)(Ev - M\dot{G}(Q)\eta - c) \tag{20b}$$

where, $\eta = \begin{bmatrix} \eta_1 & \eta_2 \end{bmatrix}^T = \begin{bmatrix} \dot{x} & \dot{y} \end{bmatrix}^T$ = pseudo-velocity

Matrix $G(q)$ has its columns in the null space of $A(q)$

$$G(Q) = \begin{bmatrix} \cos\phi & -\sin\phi \\ \sin\phi & \cos\phi \\ 0 & -\frac{1}{S} \end{bmatrix} = \begin{bmatrix} R^T \\ g_1 \end{bmatrix}; g_1 = \begin{bmatrix} 0 & -\frac{1}{S} \end{bmatrix}$$

The simplified form of Eq. (20b) is

$$\eta = \frac{mgK}{4} M_{\eta} \left[(E_1 + g_1^T e_2) + \begin{bmatrix} 2\sigma_{\Sigma} \\ \frac{W\sigma_{\Delta}}{S} \end{bmatrix} \right] \quad (21)$$

$$\text{where, } M_{\eta} = \begin{bmatrix} \frac{1}{m} & 0 \\ 0 & \frac{1}{m + \frac{I_g}{S^2}} \end{bmatrix}$$

4. SIMULATION AND RESULTS

In this section, we present the modeling response from the dynamics of UGV. In order to design the model, we follow step by step procedure and the entire simulation is done using Matlab SIMULINK. The methodology is as follows

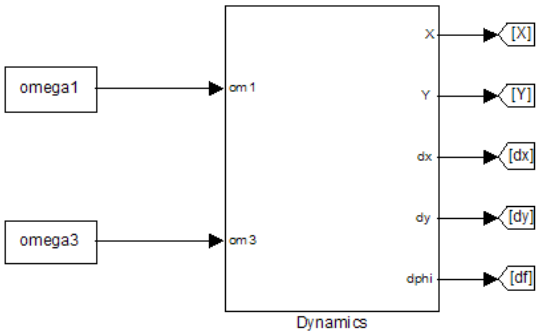

Fig. 5: SIMULINK model of the dynamic model of skid-steered UGV.

In this simulation, the UGV is designed to follow a given trajectory which is circular. For the UGV, we select: W = 0.43m, L = 0.28m, r = 0.08m, m = 5kg and I_g = 0.45kgm^2. The UGV is under constant angular velocities $\omega_1 = \omega_2$ = 60 rpm and $\omega_3 = \omega_4$ = 120 rpm. Following figure shows the trajectory response of the UGV with this wheel speed combination.

4.1 For leftward turning of UGV

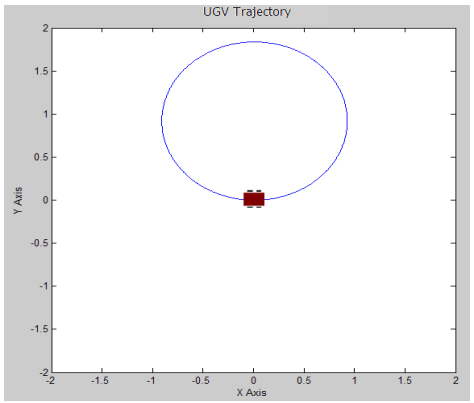

Fig. 6: UGV trajectory response.

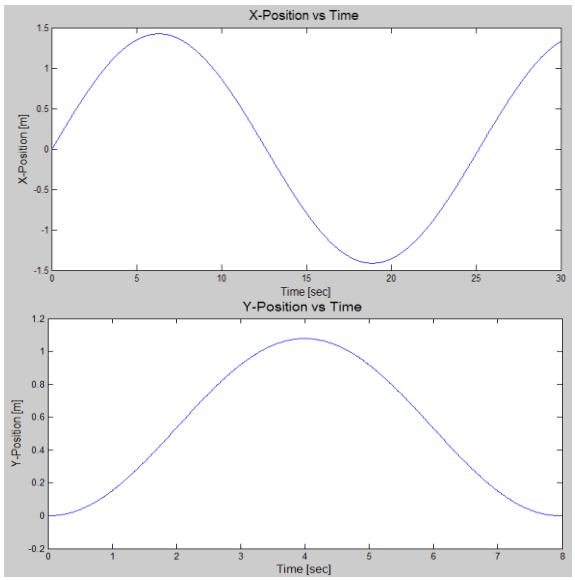

Fig. 7: Position responses.

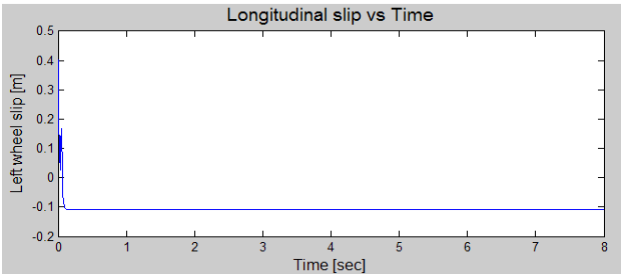

(a)

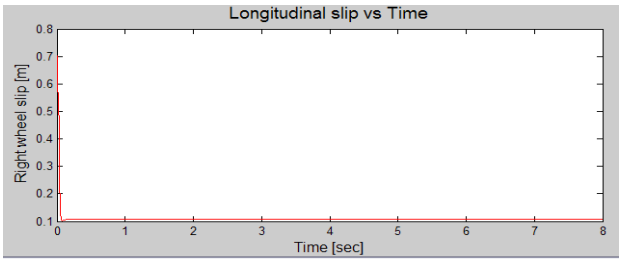

(b)

Fig. 8: Longitudinal slip for (a) left wheel = -0.107 and (b) right wheel = 0.107.

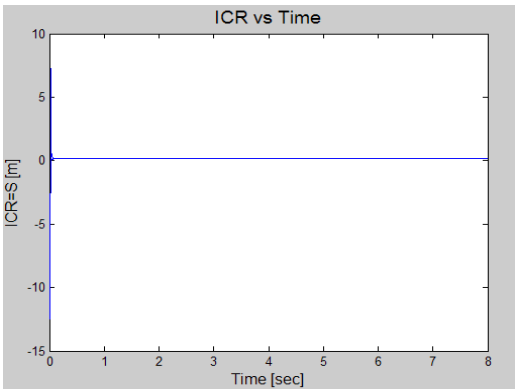

Fig. 9: Lateral skid value S = 0.152 steady after some time.

4.2 For rightward turning of UGV

If we choose opposite wheel speeds, i.e., $\omega_1 = \omega_2 = 120$ rpm and $\omega_3 = \omega_4 = 60$ rpm, the UGV is able to follow the circular trajectory of similar size and shape as follows

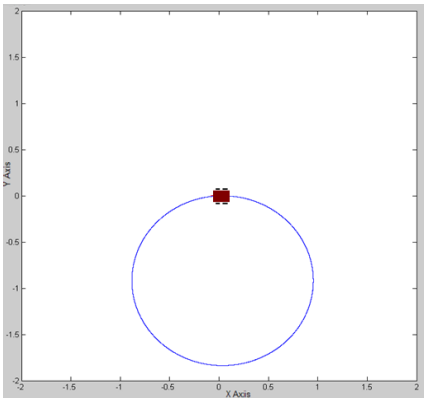

10: UGV trajectory response.

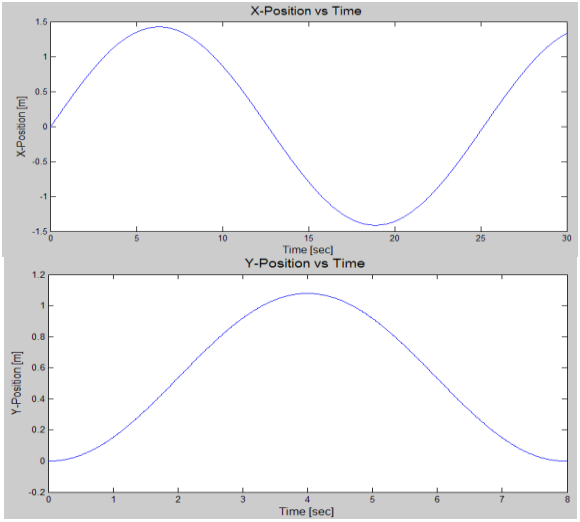

Fig. 11: Position responses.

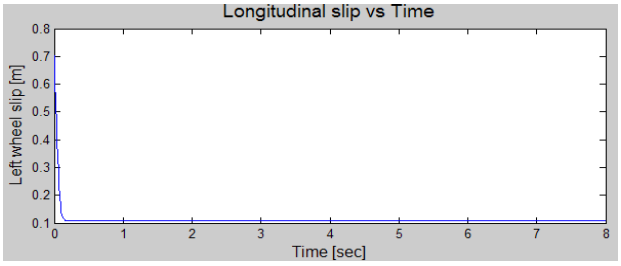

(a)

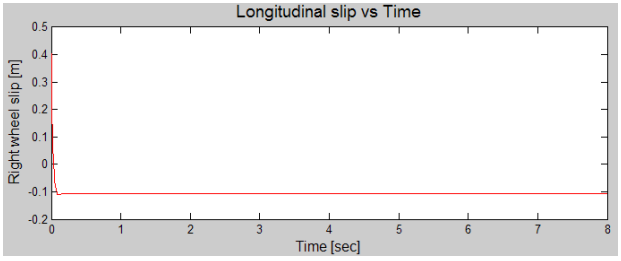

(b)

Fig. 12: Longitudinal slip for (a) left wheel = 0.107 and (b) right wheel = -0.107.

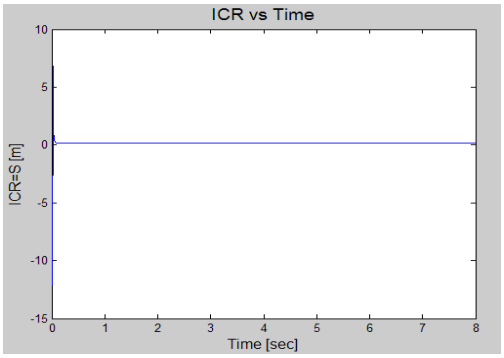

Fig. 13: Lateral skid value $S = 0.152$ steady after some time.

5. CONCLUSIONS

In this paper, a mathematical model based on the dynamics of a wheeled type skid-steered UGV was developed and then Matlab SIMULINK was used to simulate for analyzing the performance of the model. The UGV had to follow a given trajectory where wheel slipping and skidding effect were included. Both of these effects made the model distinct from other related models and a bit complex. The UGV performed quite well in making a good shaped circular trajectory with the dynamic model developed. Also the UGV gave the similar circular shaped trajectory by rotating leftwards as it did in case of the rightward turn. We also showed the wheel slipping as well as skidding effects in both cases and those effects were also similar in nature for both turns. A nonlinear slip-friction model can be included in future in order to improve the dynamic model more so that it gives better responses in rough terrains.

REFERENCES

[1] Z. Shiller and W. Serate, “Trajectory planning of tracked vehicles”, J. of Dynamic Systems, Measurement, and Control, Vol. 117, pp. 619–624, 1995.

[2] Y. Zhang, D. Hong, J. H. Chung and S. A. Velinsky, “Dynamic Model Based Robust Tracking Control of a Differentially Steered Wheeled Mobile Robot”, in proceedings of the American Control Conference Philadelphia, Pennsylvania June 1998.

[3] M. Ahmadi, V. Polotski, and R. Hurteau, “Path Tracking Control of Tracked Vehicles”, in Proc. IEEE Int. Conf. Robotics Automation, San Francisco, CA, 2000, pp. 2938–2943.

[4] L. Caracciolo, A. De Luca, and S. Iannitti, “Trajectory Tracking Control of a Four-Wheel Differentially Driven Mobile Robot”, in Proc. IEEE Int. Conf. Robotics Automation, Detroit, MI, 1999, pp. 2632– 2638.

[5] D. Wang and F. Qi, “Trajectory Planning for a Four-Wheel-Steering Vehicle”, IEEE International Conference on Robotics 8 Automation Seoul, Korea. May 21–26, 2001.

[6] K. Kozłowski and D. Pazderski, “Modeling and control of a 4-wheel skid steering mobile robot”, International Journal

of Applied Mathematics and Computer Science, Vol. 14, No. 4, pp. 101–120, 2004.

[7] J. Yi, J. Zhang, D. Song, and S. Jayasuriya, “IMU-based localization and slip estimation for skid-steered mobile robots”, in Proc. IEEE/RSJ Int. Conf. Intell. Robot. Syst., San Diego, CA, 2007, pp. 2845–2850.

[8] J. Yi, D. Song, J. Zhang, and Z. Goodwin, “Adaptive trajectory tracking control of skid-steered mobile robots”, in Proc. IEEE Int. Conf. Robot. Autom., Rome, Italy, 2007, pp. 2605–2610.

[9] D. Wang and C. B. Low, “Modeling and analysis of skidding and slipping in wheeled mobile robots: Control design perspective”, IEEE Transactions on Robotics, Vol. 24(3), pp. 676–687, 2008.

[10] R. Balakrishna and A. Ghosal, “Modeling of Slip for Wheeled Mobile Robots”, IEEE Trans. Robot. Autom., vol. 11, no. 1, pp. 126–132, 1995.

[11] J. Yi, L. Alvarez and R. Horowitz, “Adaptive Emergency Brake Control with Underestimation of Friction Coefficient,” IEEE Trans. Contr. Syst. Technol., vol. 10, no. 3, pp. 381–392, 2002.

[12] K. Weiss, “Skid-Steering,” Auto. Eng., pp. 22–25, 1971.